Title	Analysis of high-Q photonic crystal L3 nanocavities designed by visualization of the leaky components
Author(s)	Maeno, Kenichi; Takahashi, Yasushi; Nakamura, Tatsuya; Asano, Takashi; Noda, Susumu
Editor(s)	
Citation	Optics Express. 2017, 25 (1), p.367-376
Issue Date	2017-01-09
URL	http://hdl.handle.net/10466/15718
Rights	(c) 2017 Optical Society of America. Users may use, reuse, and build up on the article, or use the article for text or data mining, so long as such uses are for non-commercial purposes and appropriate attribution is maintained. All other rights are reserved.

Research Article | Vol. 25, No. 1 | 9 Jan 2017 | OPTICS EXPRESS 367
Optics EXPRESS

Analysis of high-*Q* photonic crystal L3 nanocavities designed by visualization of the leaky components

KENICHI MAENO,[1] YASUSHI TAKAHASHI,[2,*] TATSUYA NAKAMURA,[3] TAKASHI ASANO,[3] AND SUSUMU NODA[3,4,5]

[1]*Department of Applied Chemistry, Osaka Prefecture University, Sakai, Osaka 599-8531, Japan*
[2]*Department of Physics and Electronics, Osaka Prefecture University, Sakai, Osaka 599-8570, Japan*
[3]*Department of Electronic Science and Engineering, Kyoto University, Kyoto 615-8510, Japan*
[4]*Photonics and Electronics Science and Engineering Center, Kyoto University, Kyoto 615-8510 Japan*
[5]*snoda@kuee.kyoto-u.ac.jp*
[*]*y-takahashi@pe.osakafu-u.ac.jp*

Abstract: We experimentally study photonic crystal L3 nanocavities whose design *Q* factors (Q_{design}) have been improved with the visualization of leaky components design method. The experimental *Q* values (Q_{exp}) are monotonically increased from 6,000 to 2,100,000 by iteratively modifying the positions of some of the air holes, as determined by the referred design method. We investigate the Q_{exp} tolerance to imperfections in the fabricated samples, which reveals that the cavities improved by the visualization method tend to lose some tolerance to structural differences between the fabricated samples and the design values.

OCIS codes: (230.5298) Photonic crystals; (140.3948) Microcavity devices.

References and links

1. S. Noda, A. Chutinan, and M. Imada, "Trapping and emission of photons by a single defect in a photonic bandgap structure," Nature **407**(6804), 608–610 (2000).
2. Y. Akahane, T. Asano, B. S. Song, and S. Noda, "High-*Q* photonic nanocavity in a two-dimensional photonic crystal," Nature **425**(6961), 944–947 (2003).
3. B. S. Song, S. Noda, T. Asano, and Y. Akahane, "Ultra-high-*Q* photonic double-heterostructure nanocavity," Nat. Mater. **4**(3), 207–210 (2005).
4. R. Terawaki, Y. Takahashi, M. Chihara, Y. Inui, and S. Noda, "Ultrahigh-*Q* photonic crystal nanocavities in wide optical telecommunication bands," Opt. Express **20**(20), 22743–22752 (2012).
5. H. Sekoguchi, Y. Takahashi, T. Asano, and S. Noda, "Photonic crystal nanocavity with a Q-factor of ~9 million," Opt. Express **22**(1), 916–924 (2014).
6. H. Takano, B. S. Song, T. Asano, and S. Noda, "Highly efficient multi-channel drop filter in a two-dimensional hetero photonic crystal," Opt. Express **14**(8), 3491–3496 (2006).
7. Y. Takahashi, T. Asano, D. Yamashita, and S. Noda, "Ultra-compact 32-channel drop filter with 100 GHz spacing," Opt. Express **22**(4), 4692–4698 (2014).
8. T. W. Lu, P. T. Lin, K. U. Sio, and P. T. Lee, "Optical sensing of square lattice photonic crystal point-shifted nanocavity for protein adsorption detection," Appl. Phys. Lett. **96**(21), 213702 (2010).
9. S. Kita, S. Otsuka, S. Hachuda, T. Endo, Y. Imai, Y. Nishijima, H. Misawa, and T. Baba, "Photonic crystal nanolaser biosensors," IEICE Trans. Electron. **95C**(2), 188–198 (2012).
10. Y. Tanaka, J. Upham, T. Nagashima, T. Sugiya, T. Asano, and S. Noda, "Dynamic control of the Q factor in a photonic crystal nanocavity," Nat. Mater. **6**(11), 862–865 (2007).
11. J. Upham, Y. Tanaka, Y. Kawamoto, Y. Sato, T. Nakamura, B. S. Song, T. Asano, and S. Noda, "Time-resolved catch and release of an optical pulse from a dynamic photonic crystal nanocavity," Opt. Express **19**(23), 23377–23385 (2011).
12. Y. Sato, Y. Tanaka, J. Upham, Y. Takahashi, T. Asano, and S. Noda, "Strong coupling between distant photonic nanocavities and its dynamic control," Nat. Photonics **6**(1), 56–61 (2011).
13. E. Kuramochi, K. Nozaki, A. Shinya, K. Takeda, T. Sato, S. Matsuo, H. Taniyama, H. Sumikura, and M. Notomi, "Large-scale integration of wavelength-addressable all-optical memories on a photonic crystal chip," Nat. Photonics **8**(6), 474–481 (2014).
14. T. Yoshie, A. Scherer, J. Hendrickson, G. Khitrova, H. M. Gibbs, G. Rupper, C. Ell, O. B. Shchekin, and D. G. Deppe, "Vacuum Rabi splitting with a single quantum dot in a photonic crystal nanocavity," Nature **432**(7014), 200–203 (2004).

#280602 http://dx.doi.org/10.1364/OE.25.000367
Journal © 2017 Received 11 Nov 2016; revised 19 Dec 2016; accepted 19 Dec 2016; published 5 Jan 2017

Optics EXPRESS

15. K. Hennessy, A. Badolato, M. Winger, D. Gerace, M. Atatüre, S. Gulde, S. Fält, E. L. Hu, and A. Imamoğlu, "Quantum nature of a strongly coupled single quantum dot-cavity system," Nature **445**(7130), 896–899 (2007).
16. Y. Ota, M. Shirane, M. Nomura, N. Kumagai, S. Ishida, S. Iwamoto, S. Yorozu, and Y. Arakawa, "Vacuum Rabi splitting with a single quantum dot embedded in a H 1 photonic crystal nanocavity," Appl. Phys. Lett. **94**(3), 033102 (2009).
17. B. Ellis, M. A. Mayer, G. Shambat, T. Sarmiento, J. Harris, E. E. Haller, and J. Vučković, "Ultralow-threshold electrically pumped quantum dot photonic-crystal nanocavity laser," Nat. Photonics **5**(5), 297–300 (2011).
18. Y. Ota, K. Watanabe, S. Iwamoto, and Y. Arakawa, "Nanocavity-based self-frequency conversion laser," Opt. Express **21**(17), 19778–19789 (2013).
19. Y. Takahashi, Y. Inui, M. Chihara, T. Asano, R. Terawaki, and S. Noda, "A micrometre-scale Raman silicon laser with a microwatt threshold," Nature **498**(7455), 470–474 (2013).
20. Y. Akahane, M. Mochizuki, T. Asano, Y. Tanaka, and S. Noda, "Design of a channel drop filter by using a donor-type cavity with high-quality factor in a two-dimensional photonic crystal slab," Appl. Phys. Lett. **82**(9), 1341–1343 (2003).
21. Y. Akahane, T. Asano, B.-S. Song, and S. Noda, "Investigation of high-Q channel drop filters using donor-type defects in two-dimensional photonic crystal slabs," Appl. Phys. Lett. **83**(8), 1512–1514 (2003).
22. Y. Akahane, T. Asano, H. Takano, B. S. Song, Y. Tanaka, and S. Noda, "Two-dimensional photonic-crystal-slab channel -drop filter with flat-top response," Opt. Express **13**(7), 2512–2530 (2005).
23. M. Minkov and V. Savona, "Automated optimization of photonic crystal slab cavities," Sci. Rep. **4**, 5124 (2014).
24. E. Kuramochi, E. Grossman, K. Nozaki, K. Takeda, A. Shinya, H. Taniyama, and M. Notomi, "Systematic hole-shifting of L-type nanocavity with an ultrahigh Q factor," Opt. Lett. **39**(19), 5780–5783 (2014).
25. Y. Lai, S. Pirotta, G. Urbinati, D. Gerace, M. Minkov, V. Savona, A. Badolato, and M. Galli, "Genetically designed L3 photonic crystal nanocavities with measured quality factor exceeding one million," Appl. Phys. Lett. **104**(24), 241101 (2014).
26. T. Nakamura, Y. Takahashi, Y. Tanaka, T. Asano, and S. Noda, "Improvement in the quality factors for photonic crystal nanocavities via visualization of the leaky components," Opt. Express **24**(9), 9541–9549 (2016).
27. Y. Takahashi, Y. Inui, M. Chihara, T. Asano, R. Terawaki, and S. Noda, "High-*Q* resonant modes in a photonic crystal heterostructure nanocavity and applicability to a Raman silicon laser," Phys. Rev. B **88**(23), 235313 (2013).
28. A. Chutinan, M. Mochizuki, M. Imada, and S. Noda, "Surface-emitting channel drop filters using single defects in two-dimensional photonic crystal slabs," Appl. Phys. Lett. **79**(17), 2690–2692 (2001).
29. Y. Yu, M. Heuck, H. Hu, W. Xue, C. Peucheret, Y. Chen, L. K. Oxenløwe, K. Yvind, and J. Mørk, "Fano resonance control in a photonic crystal structure and its application to ultrafast switching," Appl. Phys. Lett. **105**(6), 061117 (2014).
30. Y. Takahashi, Y. Tanaka, H. Hagino, T. Sugiya, Y. Sato, T. Asano, and S. Noda, "Design and demonstration of high-*Q* photonic heterostructure nanocavities suitable for integration," Opt. Express **17**(20), 18093–18102 (2009).
31. T. Asano, B. S. Song, and S. Noda, "Analysis of the experimental *Q* factors (~ 1 million) of photonic crystal nanocavities," Opt. Express **14**(5), 1996–2002 (2006).
32. H. Hagino, Y. Takahashi, Y. Tanaka, T. Asano, and S. Noda, "Effects of fluctuation in air hole radii and positions on optical characteristics in photonic crystal heterostructure nanocavities," Phys. Rev. B **79**(8), 085112 (2009).
33. Y. Taguchi, Y. Takahashi, Y. Sato, T. Asano, and S. Noda, "Statistical studies of photonic heterostructure nanocavities with an average *Q* factor of three million," Opt. Express **19**(12), 11916–11921 (2011).

1. Introduction

High-*Q* nanocavities in two dimensional photonic crystal (PC) slabs—which possess both high quality (*Q*) factors and small modal volumes [1–5]—have attracted much attention in various fields, such as wavelength-selective filters [6,7], biosensors [8,9], optical pulse manipulation devices [10–13], solid-state cavity quantum electrodynamics [14–16], and low-threshold lasers [17–19]. In these applications, the high *Q* factors of the cavities are directly connected with desirable properties such as high resolution, high sensitivity, low operating energy, long pulse-memory time, and enhancements in nonlinear optical phenomena. Therefore, it is important to increase the *Q* factors of these cavities.

The L3 nanocavity—consisting of three missing air holes—is a very commonly used design for PC cavities [20,21]. In particular, L3 nanocavities with shifted air holes near the cavity edges are widely used in various research areas, because they can easily attain *Q* values in excess of a few tens of thousands [2,22], which are sufficient for many applications. Furthermore, L3 cavities have good connectability with PC line-defect waveguides, circular emission patterns, and small footprints [20–22]. On the other hand, their *Q* factors cannot be increased to the neighborhood of 1×10^6, a limitation that has reduced the potential of these

Optics EXPRESS

cavities. Recently, several methods have been proposed to obtain L3 cavities with design Q factors (Q_{design}) larger than several million, and experimental Q factors (Q_{exp}) larger than 1×10^6 have been reported [23–25]. The potential of L3 nanocavities has therefore been steadily increasing.

Very recently, we proposed a simple method of increasing the Q_{design} of PC cavities, to which we called visualization method [26]. It consists of the following four steps: 1) Calculate the electric-field distribution for a cavity mode, with the three-dimensional (3D) finite-difference time domain (FDTD) method; 2) Fourier transform the electric-field distribution, to determine the leaky components within the light cone, not complying with the total internal reflection condition; 3) visualize the leaky components by inverse Fourier transforming them, thus determining the particular air holes that must be shifted to increase Q_{design} in the most effective manner; and 4) modify the air-hole positions in the leaky area, so as to decrease the leaky components. It was shown that by repeating the optimization rounds from Step 1 to Step 4, the Q_{design} values for L3 cavities have been consistently increased to several million [26].

In this paper we report on the experimental evaluation of L3 nanocavities designed by the visualization method. We fabricated nine types of L3 nanocavities, using progressively higher numbers of optimization rounds. With eight optimization rounds, the Q_{exp} values were consistently increased from 6,000 to 2,100,000, whereas the values of Q_{design} increased from 6,000 to 4,200,000. We also studied the Q value dependence on the radius of the air holes; remarkable decreases in Q were obtained when the radius departed from its design value.

2. Sample structure and design Q factors

Figure 1(a) illustrates the measured samples, which consist of a triangular lattice of circular air holes on a thin silicon slab. The lattice constant a is 410 nm, and the thickness t of the slab is 217 nm. We fabricated three series of samples with different air hole radii r: 105, 110, and 115 nm; these values were confirmed by scanning electron microscopy (SEM). The excitation waveguide used to inject light into the cavity is 8% wider than the L3 cavity. Its separation (*Dis*) from the cavity is different for different samples, so that the magnitude of the evanescent mode coupling between the propagation mode and the nanocavity modes can be controlled.

Figure 1(b) shows the structure details of the fabricated L3 cavities. The red circles indicate the shifted holes after the (up to eight) optimization rounds using the visualization method, whereas the dotted circles indicate their positions before being shifted. The numbers in each circle indicate the optimization round that led to the shift of that particular air hole, and the arrows indicate the shift direction. The optimization procedure is detailed in Ref [26]. Table 1 summarizes the shift magnitudes, the calculated values of Q_{design}, and the corresponding resonant wavelengths (λ_0). In this table, the 0-round column corresponds to the normal L3 cavity, without any air hole shifts. As shown, the value of Q_{design} calculated for cavities with r = 110 nm and t = 220 nm increases monotonically from 0.006 million to 4.2 million. Although the shift magnitudes are the same of those in a previous study [26], the Q_{design} values are slightly decreased, because of the differences in the calculation parameters. We fabricated all L3 cavities (from 0-round cavities to 8-round cavities) on the same chip, with the fabrication procedure described in previous papers [4,15,19]. For comparison, we also fabricated, on the same chip, a multi-heterostructure nanocavity with a Q_{design} value of approximately 50 million [5]. The nanocavity was formed by a line defect of 17 missing air holes where the lattice constant in the x-direction was increased every two periods by 3 nm. In addition, the 8 air holes close to the cavity were shifted according to the visualization method [5]. The heterostructure nanocavity utilizes the modegap effect to confine the electric field in the x direction and therefore, the Q_{design} greater than 10 million is obtained [3,5].

Optics EXPRESS

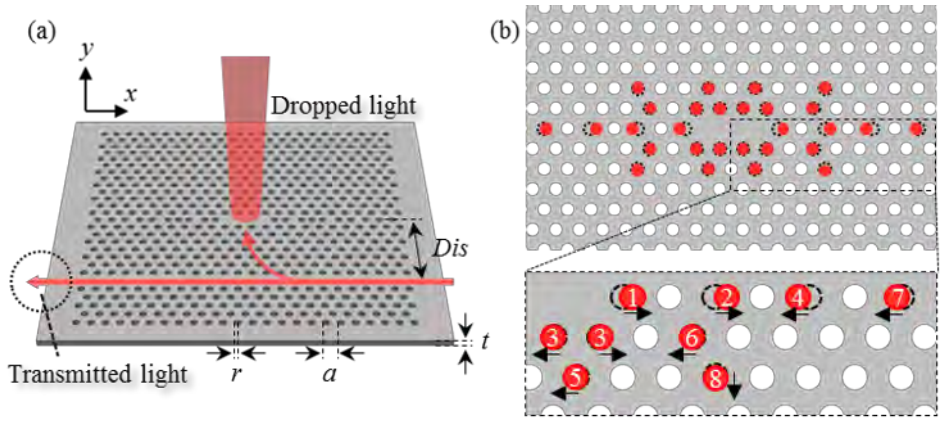

Fig. 1. (a) 3D schematic view of the samples where the L3 cavity and the excitation waveguide are formed. The light dropped from the cavity perpendicularly to the slab and the excitation waveguide transmitted light were both measured. (b) Details of the fabricated L3 cavities. The red circles indicate the shifted holes after the optimization rounds, whereas the dotted circles indicate their positions before the shift. The numbers in each circle indicate the optimization round that led to that particular shift.

Table 1. Summary results for the air hole shifts, Q_{design} values, and calculated λ_0, for nine L3 cavities with r = 110 nm. The 0-round column represents the normal L3 cavity, without air hole shifts.

Round	0	1	2	3	4	5	6	7	8
Shift magnitude (a)	–	0.2	0.23	0.015 (outer) 0.005 (inner)	0.23	0.015	0.02	0.09	0.01
Q_{design} ($\times 10^6$)	0.006	0.13	0.25	0.48	0.96	1.6	3.1	3.6	4.2
λ_0 (nm)	1550.9	1564.3	1564.5	1565.8	1565.7	1565.2	1565.0	1565.0	1565.0

3. Experiments for cavities with a 110-nm radius

3.1 Experimental results

To estimate the obtained values of Q_{exp}, we performed conventional spectral measurements on all cavities. The spectra of both the dropped and transmitted lights schematically shown in Fig. 1(a) were measured using a wavelength-tunable laser and a high-resolution wavelength meter. Details of the experiment were described in a previous paper [27]. Figures 2(a)-2(i) show the results obtained for the nine L3 cavities (from the 0-round to 8-round cavities respectively), with r = 110 nm. The experiment was performed at room temperature, in standard air atmosphere. The black open circles in these figures represent the experimental data obtained for the dropped light, whereas the red curves show the transmitted spectra. The black solid curves are fitted curves (Lorentzian functions) used to evaluate λ_0 and the full width at half maximum ($\Delta\lambda_{FWHM}$). The shape of the drop spectrum in Fig. 2(a) is not symmetric because of the Fabry-Perot oscillation of the excitation waveguide. The blue curve represents the drop spectrum divided by the transmitted spectrum, which roughly reproduces an intrinsic resonant peak. The Q_{exp} values for the 0-round to 7-round cavities were estimated using the following relation [28]:

$$Q_{exp} = \frac{\lambda_0}{\Delta\lambda_{FWHM}\sqrt{T_0}}, \quad (1)$$

Optics EXPRESS

where T_0 is the transmittance at the resonant peak.

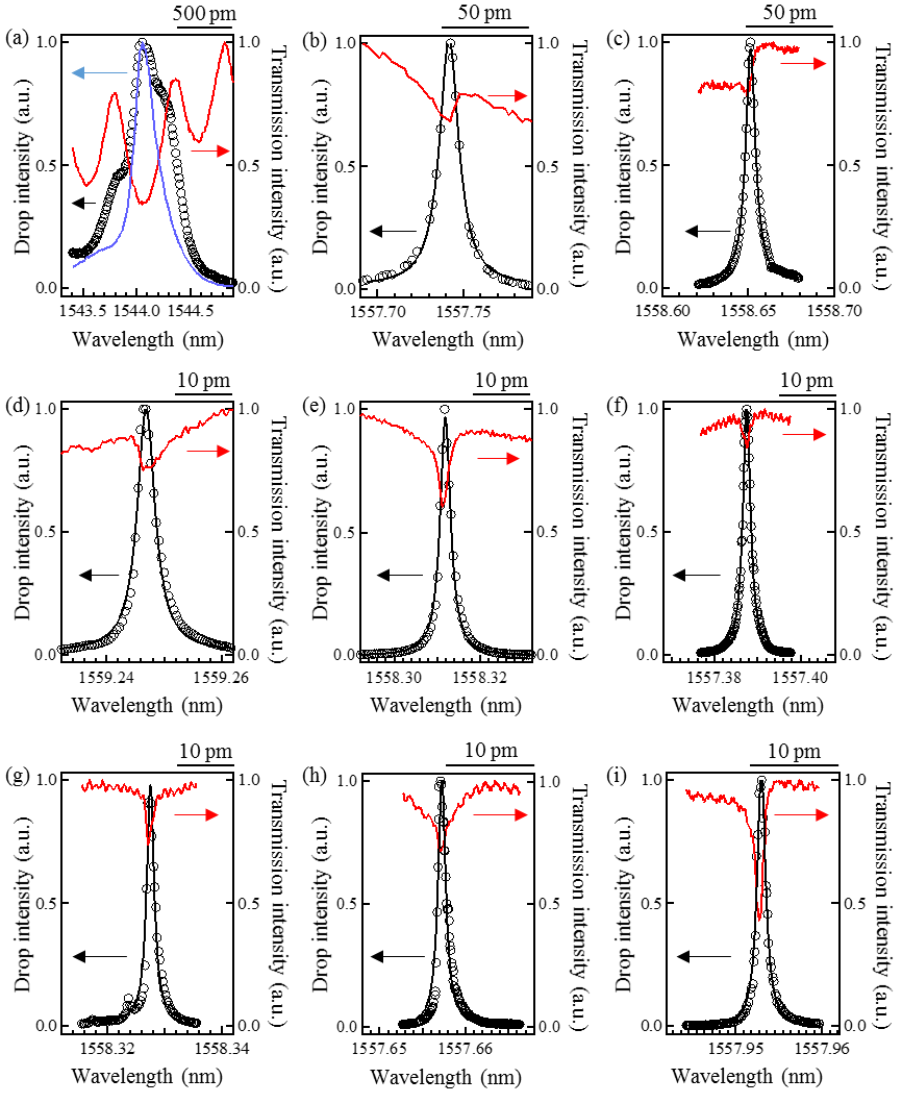

Fig. 2. (a)–(i) Dropped and transmitted spectra for the 0- to 8-round L3 nanocavities, respectively. Black circles represent the experimentally obtained results for the dropped light, whereas the red curves are the transmitted spectra. The black solid curves show the fitted Lorentzian functions. The blue curve in Fig. 2(a) is the drop spectrum divided by the transmitted spectrum.

In the spectral measurements, a temperature variation of the sample as small as 0.01 K may shift λ_0 by as much as 0.8 pm. In addition, the Fano effect causes the asymmetric shapes of the drop peak and transmission dip [29]. These factors result in non-negligible error in the $\Delta\lambda_{FWHM}$ determination. Therefore, to correctly evaluate the highest Q_{exp}, we used a time-domain approach to the measurements of the 8-round cavity. In the measurement, 5-ns-wide rectangular light pulses were applied to the excitation waveguide, and the time-domain evolution of the emissions from the cavity was measured using a photomultiplier tube and a time-correlated single-photon counting method. The experiment was also performed in standard air. Details of the measurement have been previously described in [5,30].

Optics EXPRESS

Figure 3 shows the time response of the 8-round L3 cavity, which indicates a photon lifetime τ of 1.15 ns for the cavity. Q_{exp} was then estimated using the following relation:

$$Q_{exp} = \frac{\omega_0 \tau}{\sqrt{T_0}}, \tag{2}$$

where ω_0 is the angular frequency and T_0 is the transmittance obtained from the spectral measurement.

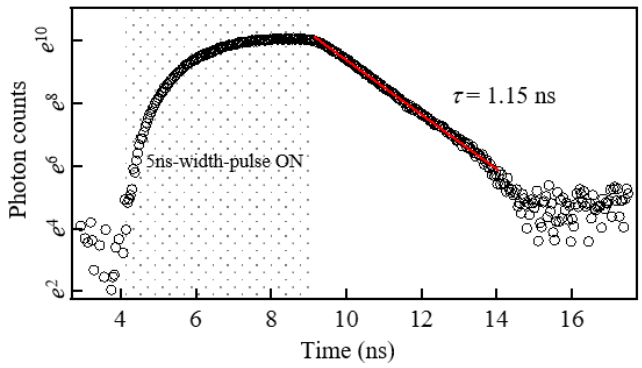

Fig. 3. Time-resolved signals for the nanocavity, with a 5-ns-wide pulsed light input. The shaded region corresponds to the pulsed input ON interval. The red fitted line indicates a 1.15 ns photon lifetime.

Table 2 summarizes the experimental results obtained with the nine L3 cavities. The λ_0 shifts by 14 nm from round 0 to round 1, whereas it rarely changes from round 1 to round 8. This behavior agrees with the calculated results shown in Table 1. The value of Q_{exp} increases monotonically with the increase in the number of optimization rounds. It exceeds one million with six rounds, and reaches 2.1 million with eight rounds. This value is comparable to the highest Q_{exp} values ever reported for L3 cavities [25], and clearly demonstrates that the visualization method is useful for designing high-Q PC cavities.

Table 2. Summary measured results for the nine nanocavities: resonant wavelength (λ_0), linewidth ($\Delta\lambda_{FWHW}$), transmittance (T_0), distance between the cavity and the excitation waveguide (*Dis*), and experimental Q factor (Q_{exp}). The Q_{exp} values for the 8-round and multi-hetero (MH) nanocavities are estimated from the photon lifetime obtained from time-domain measurements.

Round	0	1	2	3	4	5	6	7	8	MH
λ_0 (nm)	1544.1	1557.7	1558.7	1559.3	1558.3	1557.4	1558.3	1557.7	1558.0	1576.5
$\Delta\lambda_{FWHM}$ (pm)	246	13.7	7.14	3.83	2.91	2.16	1.56	1.09	(1.15 ns)	(3.80 ns)
T_0	–	0.81	0.89	0.84	0.65	0.88	0.75	0.72	0.46	0.95
Dis ($\sqrt{3}a$)	3.5	3.5	3.5	3.5	4.5	4.5	4.5	4.5	4.5	4
Q_{exp} ($\times 10^6$)	0.006	0.13	0.23	0.44	0.66	0.77	1.2	1.7	2.1	4.7
Q_{imp} ($\times 10^6$)	–	–	–	–	2.1	1.5	2.0	3.2	4.2	5.1

Optics EXPRESS

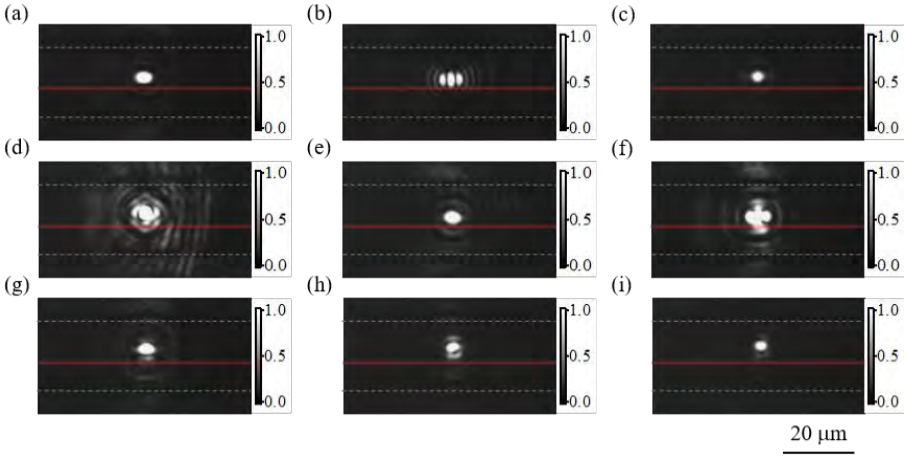

Fig. 4. (a)–(i) Near-infrared camera images of the 0-round to 8-round L3 cavities, respectively. The red lines represent the waveguides; the dashed lines indicate the PC pattern region interfaces.

Figures 4(a)-4(i) show near-infrared camera images for the 0- to 8-round cavities, respectively. A single-lobed spot was obtained for the normal (0-round) L3 cavity, and a sidelobed spot was obtained for the 0.2 *a*-shifted 1-round L3 cavity, which is in good agreement with previously published studies [7,21]. Single-lobed spots were obtained for many cavities. Some distorted and split spots seem to be random effects resulting from the stochastic nature of the scattering caused by air hole fluctuations in radius and position, because they have not been reproduced in experiments with different samples.

3.2 Discussion for discrepancy between Q_{exp} and Q_{design}

The discrepancy between Q_{exp} and Q_{design}—which is caused by the additional loss factors (Q_{imp}) resulting from imperfections in the fabricated samples—should now be discussed [5,31–33]. The three Q factors are related by:

$$\frac{1}{Q_{\mathrm{exp}}} = \frac{1}{Q_{\mathrm{design}}} + \frac{1}{Q_{\mathrm{imp}}}. \tag{3}$$

The reciprocal Q values are the optical losses. For cavities with $1/Q_{\mathrm{design}} \gg 1/Q_{\mathrm{imp}}$, Q_{exp} should be approximately equal to Q_{design}. Such results are obtained for the 0- to 3-round cavities. The discrepancy becomes prominent for cavities with $1/Q_{\mathrm{design}} \cong 1/Q_{\mathrm{imp}}$, which corresponds to the 4- to 8-round cavities. The Q_{imp} values for these cavities derived from Eq. (3) are also presented in Table 2, and are distributed between 1.5 and 4.2 million.

We also measured the Q_{exp} values of 10 multi-heterostructure nanocavities fabricated on the same chip with a = 410 nm and r = 110 nm, using time-domain measurements. All the cavities possessed Q_{exp} values above 4.0 million; an average Q_{exp} value of 4.7 million was obtained, corresponding to a Q_{imp} value of 5.1 million, as results from Eq. (3). These results are also presented in Table 2. Since both types of nanocavities were fabricated on the same chip, the magnitudes of the imperfections must be the same. However, the values of Q_{imp} for the L3 cavities are lower than those for the heterostructure nanocavity and the variation of Q_{imp} for the L3 cavities seems to be large. These inconsistencies suggest that the L3 cavities designed with the visualization method lose tolerance to some structural imperfections.

Then, we performed 3D FDTD simulations to take the possibility of air-hole variations into account [32]. Normally distributed random nanometer-scale variations in position and radius were applied to all the air holes, with a standard deviation of σ_{hole} = 1 nm. The average

Optics EXPRESS

value of $1/Q_{imp}$ obtained for 30 different fluctuation patterns were almost identical for the 6-, 7-, and 8-round cavities: 8.91×10^{-7}, 8.90×10^{-7}, and 8.88×10^{-7}, respectively. The standard deviation of $1/Q_{imp}$ were also equal for the three cavities: 4.26×10^{-7}, 4.26×10^{-7}, and 4.19×10^{-7}, respectively. On the other hand, the average value and the standard deviation for the multi-heterostructure nanocavity are 6.91×10^{-7} and 3.03×10^{-7}, respectively, which are somewhat smaller than the L3 cavities. These indicate that the L3 cavities have slightly lower tolerance to random structural disorders. However, it does not give a sufficient explanation for the inconsistencies of Q_{imp} values shown in Table 2. Another cause will be discussed below.

4. Dependence of Q on the air hole radius

4.1 Experimental results

In this section, we will focus on the dependence of Q on the air hole radius. In fact, it is very difficult to fabricate PC samples with a given target radius with accuracies of (or above) 1 nm (e.g., $r = 110 \pm 1$ nm). This is because the final obtained radius is affected by several of the fabrication steps, such as electron beam lithography, development, and plasma etching. Furthermore, the radius of a fabricated PC sample is determined by SEM observations, whose accuracy is of only a few nm. Therefore, the dependence of Q on the radius is a core component of the tolerance to structural imperfections.

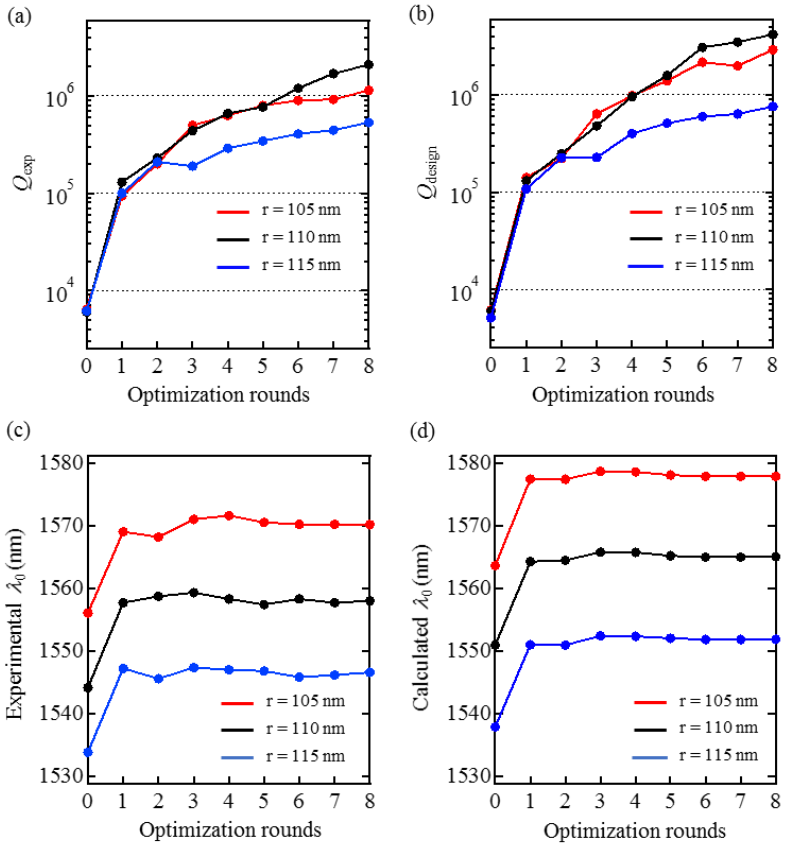

Fig. 5. (a) Experimental Q factors, and (b) calculated Q factors for three series of L3 cavities. (c) Experimentally obtained resonant wavelengths. (d) Calculated resonant wavelengths. The red dots, black dots, and blue dots represent cavities with r = 105, 110, and 115 nm, respectively.

Optics EXPRESS

We fabricated three different series of L3 cavities, with radii of 105, 110, and 115 nm. They have the same values for air hole shifts as those shown in Table 1. Figure 5(a) shows the corresponding values of Q_{exp}. As shown, up to round 2, the value of Q_{exp} is approximately the same in all three cases. In round 3, the cavity with r = 115 nm exhibits a lower value than the other two, and the gap either increases or is maintained with the following rounds; the maximum value of Q_{exp} for r = 115 nm is as small as 530,000, even in round 8. The cavity with r = 105 nm has a smaller value in round 6 than the cavity with r = 110 nm, and this gap increases in the following rounds; a maximum value of 1,140,000 is reached in round 8. Figure 5(b) presents the calculated values for Q_{design} using the 3D FDTD method; as can be seen, these results are consistent with the experimental results. Figures 5(c) and 5(d) present the experimentally obtained values of λ_0 and their corresponding calculated values, respectively. As shown, they are in good agreement. The slight shifts in the absolute values can originate from small differences in radii and refractive index between experiments and calculations.

4.2 Discussion for tolerance to structural design differences

Table 3 summarizes the results obtained for Q_{exp} and Q_{design}. It should be noted that the ratio of Q_{design} for r = 115 nm and Q_{design} for r = 110 nm is 0.91 in round 0, and decreases to 0.17 in round 8. Similarly, the ratio of Q_{design} for r = 105 nm and Q_{design} for r = 110 nm is 1.09 in round 0, decreasing to 0.51 in round 8. In general, the Q_{design} values for PC cavities increase with a decrease in the air hole radius. This is because the effective refractive index relative to the cavity mode field increases when the radius decreases, which enhances the light confinement by total internal reflection. The calculated results for a normal two-step heterostructure nanocavity with a_1 = 410 nm, a_2 = 415 nm, and a_3 = 420 nm [3] are shown in Table 3. The Q_{design} values for the 110 and 115 nm radii are almost identical, with the Q_{design} for r = 105 nm being greater than those two. On the other hand, the L3 cavities with r = 105 nm have smaller values of Q_{design} when compared to the cavities with r = 110 nm, for several numbers of rounds. It can therefore be concluded that the L3 cavities improved by the visualization method tend to decrease the tolerance to differences between the air hole radii of the fabricated samples and their design values. A similar tendency could be seen in the L3 cavities designed by the genetic optimization method [23]. Therefore, we suspect that this may be a universal characteristic of the improvement methods based on air hole shifts.

The value of Q_{design} is also influenced by differences in the slab thickness. The ratio of Q_{design} for t = 215 nm and Q_{design} for t = 220 nm is 0.98 in the 0-round L3 cavity with r = 110 nm. The normal two-step heterostructure nanocavity also exhibits the same ratio. On the other hand, this ratio decreases to 0.89 in the 8-round L3 cavity. The shift and Q_{design} values shown in Table 1 were calculated using r = 110 nm and t = 220 nm, whereas the measured samples have t = 217 nm. Furthermore, as discussed above, the radii have an uncertainty of a few nm, owing to SEM resolution limitations. These can be the main causes of the smaller Q_{imp} and the large variation observable in Table 2. The inconsistency between the refractive index used in the calculations and the one of the fabricated samples must also be considered in this discussion, because it will generate some errors in the optimal positions of the air holes.

The Q_{exp} does not seem to have reached saturation even with eight rounds as shown in Table 2. Additional optimizations via the visualization method would therefore further increase the highest Q_{exp}. However, we need to feedback the experimental results into the design calculation to adjust the differences between the calculations and the fabricated samples.

Optics EXPRESS

Table 3. Summary results for Q_{exp} (upper row) and Q_{design} (lower row) for the nine L3 cavities and multi-hetero nanocavities (MH), with different air hole radii: 105, 110, and 115 nm.

Round	0	1	2	3	4	5	6	7	8	MH
Q (× 10^6)	0.006	0.09	0.20	0.50	0.63	0.80	0.90	0.92	1.1	–
r = 105 nm	0.006	0.14	0.22	0.64	0.98	1.4	2.2	2.2	2.1	21.2
Q (× 10^6)	0.006	0.13	0.23	0.44	0.66	0.77	1.2	1.7	2.1	–
r = 110 nm	0.006	0.13	0.25	0.48	0.96	1.6	3.1	3.6	4.2	16.1
Q (× 10^6)	0.006	0.10	0.21	0.19	0.29	0.34	0.41	0.45	0.53	–
r = 115 nm	0.005	0.11	0.23	0.23	0.40	0.51	0.60	0.63	0.70	16.0

5. Conclusion

We demonstrated that the visualization method is useful for designing high-Q PC cavities. Repeating the optimization round eight times, the Q_{exp} values of the L3 cavities were monotonically increased from 6,000 to 2,100,000. We also investigated the tolerance of the resulting Q factors to structural imperfections. It was shown that these L3 cavities tend to lose tolerance to structural differences in design, especially in what concerns the air hole radius. Our results show that the values of Q_{exp} about one million can be constantly obtained in the L3 cavities. Application area of L3 cavity will further extend.

Funding

JSPS KAKENHI (15H05428, 15K13326); Toray Science Foundation; Asahi Grass Foundation; CPHoST program; New Energy and Industrial Technology Development Organization (NEDO).

Acknowledgment

K. Maeno was given the occasion to study the high-Q nanocavities by the SiMS program for Leading Graduate Schools.